Evaluation of Force Controllers for a Gravity-Compensating Upper Limb Soft Exoskeleton

by

Jaeyong Song

to obtain the degree of Master of Science
at the Delft University of Technology,
to be defended publicly on Tuesday October 29, 2019 at 10:00 AM

Student number:	4743164	
Thesis committee:	Dr. -Ing. H. Vallery,	TU Delft, supervisor
	Dr. A. A. Zadpoor	TU Delft
	S. Jabeen	TU Delft
External Supervisor:	A.-M. Georgarakis,	ETH Zürich, supervisor
	Dr. M. Xiloyannis,	ETH Zürich, supervisor

This thesis is confidential and cannot be made public until June 30, 2021.

An electronic version of this thesis is available at http://repository.tudelft.nl/

Mechanical, Maritime and Materials Engineering (3mE)
Delft University of Technology
The Netherlands

Table of Contents

Abbreviations

ADL	Activities during Daily Living
DF	Direct Force
DFF	Direct Force with Friction Compensation
EMG	ElectroMyoGraphy
FS	Force Sensor
G/A	Gravity Assistance
IF	Indirect Force
IMU	Inertial Measurement Unit
MJT	Minimum Jerk Trajectory
MCU	MicroController Unit
RMSE	Root Mean Square Error
SD	Standard Deviation
SPARC	SPectral ARC length

Abstract

For assistive exoskeletons, researchers have introduced soft exoskeletons (exosuits) because they tend to be lightweight, easily worn and mobile for daily use. However, most existing devices have not introduced closed-loop control methods that users can intuitively learn and use during activities of daily living.

The goal of this pilot study is to design and test adequate controllers on the shoulder exosuit for the main study with human trials. In this paper, three controllers, namely a direct force (DF) controller, a direct force controller with a friction compensation (DFF) and an indirect force (IF) admittance controller, are introduced and tested for their feasibility and performance on the exosuit on a human.

The controllers were initially tested on the test bench and the DF and IF controllers were selected and compared to a no-controller condition as a pilot study on the exosuit with four participants. Three different conditions did not show significant difference in tracking error, smoothness and bandwidth in arm elevation. However, the IF controller showed better performance in force than the DF controller for the tracking error of $2.95 \pm 0.15\,\mathrm{N}$ (mean$\pm$standard deviation) and $9.34 \pm 2.99\,\mathrm{N}$, and for the smoothness of movements (SPectral ARC length) of -4.70 ± 0.61 and -7.07 ± 0.89, respectively. The force error between reference and measured force noticeably increased from 0.5 Hz of elevation movements which is similar to their force bandwidth of 0.55 Hz for the IF controller and 0.4 Hz for the DF controller.

Despite the fact that the obtained results may not suffice to verify that the controllers provide sufficient assistance to a user, the indirect force admittance controller with the given experiment procedure shows promising results and performance with the exosuit which can later be used for further studies and human trials.

ME51032 ME-BMD MSc Project
J. Song (4743164), TU Delft, The Netherlands

Evaluation of Force Controllers for a Gravity-Compensating Upper Limb Soft Exoskeleton

Jaeyong Song[1], Anna-Maria Georgarakis[2] and Michele Xiloyannis[2]

***Abstract*—For assistive exoskeletons, researchers have introduced soft exoskeletons (exosuits) because they tend to be lightweight, easily worn and mobile for daily use. However, most existing devices have not introduced closed-loop control methods that users can intuitively learn and use during activities of daily living. The goal of this pilot study is to design and test adequate controllers on the shoulder exosuit for the main study with human trials. In this paper, three controllers, namely a direct force (DF) controller, a direct force controller with a friction compensation (DFF) and an indirect force (IF) admittance controller, are introduced and tested for their feasibility and performance on the exosuit on a human. They were initially tested on the test bench and the DF and IF controllers were selected and compared to a no-controller condition as a pilot study on the exosuit with four participants. Three different conditions did not show significant difference in tracking error, smoothness and bandwidth in arm elevation. However, the IF controller showed better performance in force than the DF controller for the tracking error of $2.95 \pm 0.15\,\mathrm{N}$ (mean±standard deviation) and $9.34 \pm 2.99\,\mathrm{N}$, and for the smoothness of movements (SPectral ARC length) of -4.70 ± 0.61 and -7.07 ± 0.89, respectively. The force error between reference and measured force noticeably increased from 0.5 Hz of elevation movements which is similar to their force bandwidth of 0.55 Hz for the IF controller and 0.4 Hz for the DF controller. Despite the fact that the obtained results may not suffice to verify that the controllers provide sufficient assistance to a user, the indirect force admittance controller with the given experiment procedure shows promising results and performance with the exosuit which can later be used for further studies and human trials.**

I. Introduction

OVER the past years, the amount of research and development in exoskeletons has increased due to their potential benefits and their possible applications for various purposes, namely rehabilitation, assistance and augmentation. Eighty-five percent of the upper limb exoskeletons described in recent studies were focused on the rehabilitation and assistance purposes as shown in Fig.1(a) [1]–[8].

Rehabilitation exoskeletons are mostly used for supporting patients with neuromuscular disorders, for example, muscular injuries, myopathy and stroke, in exercises while reducing physical burden on therapists. Most of the devices are constructed with rigid frames due to precise force delivery at each desired supported joint [9]–[14]. One of the significant drawbacks in the past was misalignment at the actuated joints which could be resolved by introducing self-aligning mechanisms [12]–[14]. However, self-alignment systems can make the devices more complex and heavier. The additional weight to the devices can result in an increase of a metabolic cost for the users especially when the robots are made portable [15], [16]. In addition, because the devices are often used in restricted environments such as rehabilitation centres or clinics, they generally lack mobility that limits their use for assistance applications [9], [12]–[14]. These drawbacks make them unsuitable for assisting people in daily life. Therefore, researchers have looked for other solutions.

The upper limb exoskeletons for assistance have gathered research interest due to an aging society and individual's

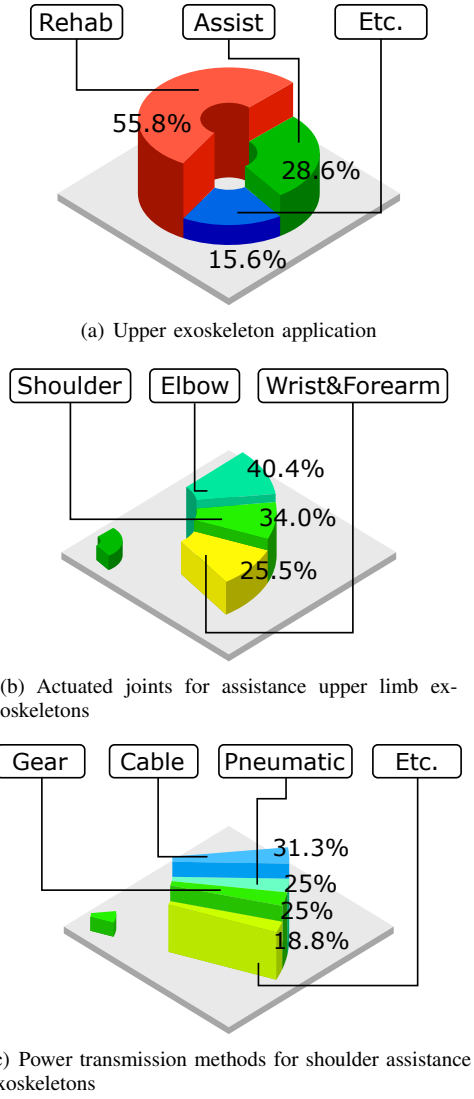

(a) Upper exoskeleton application

(b) Actuated joints for assistance upper limb exoskeletons

(c) Power transmission methods for shoulder assistance exoskeletons

Fig. 1. Classification of upper limb exoskeletons based on (a) application (b) supported joint in recent publications [1]–[8]. (c) Relative proportions of power transmissions for shoulder exoskeletons.

[1]J. Song is with Mechanical, Maritime and Materials Engineering (3mE), Delft University of Technology (TU Delft), 2628 CD Delft, The Netherlands (email: J-Song.2@student.tudelft.nl).

[2]A.-M. Georgarakis and M. Xiloyannis are with the Sensory-Motor Systems Lab, ETH Zürich, 8092 ETH Zürich, Switzerland (email: marie.georgarakis@hest.ethz.ch, michele.xiloyannis@hest.ethz.ch).

well-being [1], [17]. Many studies have explored suitable applications for assistance exoskeletons and introduced soft exoskeletons (exosuits) because of their many advantages [2]–[4], [7], [8], [18]–[20]. Exosuits are made of compliant materials or fabrics which make them portable and lightweight. These devices rely on the musculoskeletal system of the user as a rigid structure to transmit forces, causing no misalignment at actuated joints [21].

In the recent past, several soft exosuits have been developed for daily assistance of the upper extremities. Some approaches for the shoulder assistance showed reductions in electromyography (EMG) signals of the muscles responsible for elevating the arm [2], [3], [19]. However, these results were obtained with open-loop controllers on the assistive devices. For practicable use in daily life, assistive devices need to be intuitively controllable by the user, or follow the user's movements as needed. In addition, some applications were still light-weight and hence not mobile [3], [9], [18], [22]. Recent studies in elbow exosuits introduced more compact and wearable devices with closed-loop controllers that assist general movements in the elbow joint [6], [7]. It suggests the potential that a shoulder exosuit can also be wearable and automated with such control strategies to assist general movements at the shoulder joint when needed. Thus, here we present Myoshirt, a wearable shoulder exosuit with a closed-loop controller.

The Myoshirt, illustrated in Fig.2, is a garment-like exosuit with a cable-driven actuation system that assists arm elevation movements. Cable-driven power transmission has its benefit of being able to deliver force from a distal power source and electric motors are the most commonly used power source for assistive exoskeletons as shown in Fig.1(c).

In this paper, the technical requirements for an effective controller for a shoulder exosuit were derived then three different controllers for a cable-driven actuation system were designed and tested on a customized test bench. Then two controllers were selected and evaluated with the exosuit on the research members in the lab as a pilot test. Based on the test results, one controller was recommended for the main study. In addition, some suggestions for improvements in the controller and the experiment procedure were discussed.

The definition of the joint coordinate systems and rotations used in the methods follows the ISB recommendation [23].

II. Methods

A. Requirements

The aim of the Myoshirt is to assist arm elevation for the elderly and individuals with muscular weakness in the shoulder. The healthy elderly or individuals with muscular weakness can still perform activities of daily living (ADLs) but they get tired more easily than when they were younger. Thus, some supplementary assistance during ADLs can be beneficial allowing the elderly to remain more active and independent for a longer period of time, resulting in better quality of living. To assist the movements, the device is required to generate sufficient force. In addition, the device should not interfere with the natural movements of the user.

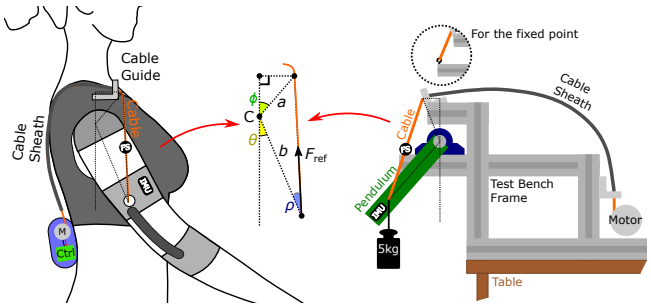

Fig. 2. A simplified model of an exosuit with the human and the test bench that resembles the model. The model was used to estimate a required pulling force from the motor. The cable guide is a rigid component of the exosuit where the cable sheath is connected from the motor system.

To facilitate gravity compensation, the sum of required torque from the motor, τ_{ref}, and torque that a user contributes to hold his/her arm still, τ_{h}, should be equal to the gravitational torque at the shoulder joint, τ_{g}:

$$\tau_{\mathrm{g}} = \tau_{\mathrm{ref}} + \tau_{\mathrm{h}}. \tag{1}$$

Using a simple model of the exosuit on the human as shown in Fig.2, the required cable tension for gravity compensation can be estimated. Based on the model and assumption that the cable guide does not move, the required cable tensile force, F_{ref}, can be expressed as

$$\begin{aligned} \tau_{\mathrm{ref}} &= b\,\sin(\rho)\,F_{\mathrm{ref}} \\ \rho &= \mathrm{acos}\left(\frac{b + a\,\cos\left(\phi+\theta\right)}{\sqrt{a^2+b^2+2\,a\,b\,\cos\left(\phi+\theta\right)}}\right) \\ F_{\mathrm{ref}} &= \frac{\tau_{\mathrm{g}} - \tau_{\mathrm{h}}}{b\sqrt{1-\frac{(b+a\,\cos(\phi+\theta))^2}{a^2+b^2+2\,a\,b\,\cos(\phi+\theta)}}} \end{aligned} \tag{2}$$

where C is the center of rotation of the upper arm at the shoulder joint, a the distance from C to the distal tip of the cable guide, b the distance from C to the point where the cable is tethered, θ the arm elevation angle, ϕ the angle between the vertical line from C and the line from C to the distal tip of the cable guide and ρ the angle between the upper arm and the cable as shown in Fig. 2. The gravitational torque, τ_{g}, can be obtained using anthropometric data of a user. When the user is fully supported by the robot, τ_{h} will converge to zero.

Exosuits must be transparent so as to not interfere with the natural movements of the users. The user intention detection is of paramount importance to make the devices transparent [24]. Also, the device must have sufficient bandwidth to cover the frequency bandwidth of arm elevation movements so that it will be able to accommodate general shoulder movement speeds of users in daily life. If we approximate the shoulder elevation movement as a single sinusoidal trajectory, the trajectory and angular speed of the movement can be defined as

$$\begin{aligned} \theta &= \theta_0 + \theta_1 \sin(2\pi f t) \\ \dot{\theta} &= 2\pi\,\theta_1\,f\cos(2\pi f t) \end{aligned} \tag{3}$$

where θ is an arm elevation angle, $\dot{\theta}$ is an arm elevation angular velocity, θ_0 is 50°, θ_1 is 40° and f is a frequency of the arm

movement at a given cycle. The angles, θ_0 and θ_1, were chosen to cover the range of motion during most of ADLs.

Arm elevation angles of ADLs range from 20° to 120° with average of 68° [25]–[29] and the average angular velocity of arm elevation varies from $30.4\,^\circ\,\mathrm{s}^{-1}$ to $91.2\,^\circ\,\mathrm{s}^{-1}$ in a slow to fast movement, respectively [30]. Assuming that people move their arm with minimum jerk trajectory (MJT) [31], the peak velocity of the arm elevation is $168\,^\circ\,\mathrm{s}^{-1}$ for the fast movement speed. With the above reference values substituted in (3), the minimum required bandwidth to support a fast arm elevation is 0.67 Hz.

In conclusion, the actuation system is required to generate sufficient force based on (2). Also, the system must have a higher bandwidth than 0.67 Hz in order to support high arm elevation speed for better transparency of the device.

B. Test Bench & Actuation System Setup

Because the human is an inherent part of the system, there are enormous safety concerns when testing the device directly on the human. Three controllers were firstly tested on a test bench that resembles the simplified model of the shoulder joint shown in Fig.2.

The test bench consists of a cable driven actuation system, a fixed point or a pendulum with bearings, that is a simplified model for an upper arm with the shoulder joint, and electric components as shown in Fig 2.

A schematic diagram of actuation is shown in Fig.3. The system is composed of a brushless electric motor (Maxon, EC-i 40, 100W) combined with a reduction gear (Maxon, GP42, 26:1) and a spool ($\varnothing 34\,\mathrm{mm}$) connected to the motor's shaft. In this configuration, the actuation system can generate up to $220\,\mathrm{N}$ in a continuous operation mode. The force is delivered through a cable (Dyneema cable / Dyneema-PES cable, $\varnothing 1.25\,\mathrm{mm}$) tethered from the spool to an end-effector. A microcontroller unit (MCU) (NXP, FRDM-K66F) is used to send control commands out at 1 kHz to a motor controller (Maxon, ESCON 50/5) that can control either torque or speed of the motor. An inertial measurement unit (IMU) (Hillcrest Laboratories, FSM300) is attached to the pendulum to measure the elevation angle. Accuracy of the IMU was validated with a motion capture system and a rotary encoder as shown in Appendix C. A load cell (Futek, LSB200, $445\,\mathrm{N}$) with a voltage amplifier (Futek, IAA100) is connected at the end effector in series with the cable to measure the applied force at the end effector.

Based on the geometry of the test bench, mass of the pendulum and (2), the maximum required cable pulling force is 115 N for a pendulum elevation angle from 0° to 90° which lies within the motor's capabilities. However, the required force at the end effector is dependent on the geometry of a system and losses due to inertia, elasticity, deformation, friction and so on. Thus, the required force at the end effector for the exosuit will differ from the obtained value above. Nevertheless, the maximum required force on the exosuit is expected to reside below 150 N [3], [32]. Therefore, it is valid to infer properties of the exosuit from the results of the evaluation on the test bench.

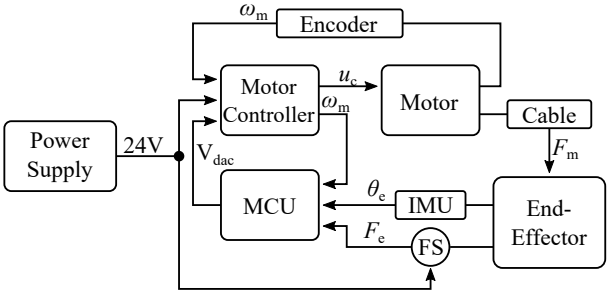

Fig. 3. A schematic diagram for the actuation system. MCU is a microcontroller unit, IMU is an inertial measurement unit and FS is a force sensor. The end-effector is either a fixed point, a pendulum or an exosuit depending on the experiments. The MCU is responsible for control and sends out a control signal to the motor controller. Then the motor controller controls either speed or current of the motor that generates force through a cable tethered to the end-effector. The measurement units, namely IMU and the force sensor, measure an elevation angle and an applied force which are collected by the MCU. The motor controller and the force sensor were powered with 24 V. (ω_m: the speed of motor in revolutions per minute, u_c: the control signal between the motor controller and the motor, V_dac: the control signal between MCU and the motor controller, F_m: the assistive force, θ_e: the measured elevation angle, F_e: the measured assistive force.)

C. Controllers

Controllers for assistive exosuits should be capable of compensating gravity of the upper extremity without interfering with the user's natural movements. Based on these requirements, three different controllers were implemented. Two of them are PI force controllers and the other is a PI admittance controller as illustrated in Fig. 4.

All three controllers comprise some components in common such as the gravity assistance estimator (G/A estimator), the motor system, the exosuit and human. In order to compensate gravity at the shoulder joint, the G/A estimator was introduced to estimate a required force at the end-effector. Equation (2) was used for the G/A estimator and the estimator was tuned for each participant.

Even though the three controllers have some components in common, they have their own features to control the force at the end-effector. All controllers were running at 1 kHz for the experiment.

1) Closed-Loop Direct Force Controller: A PI controller was implemented to design the direct force (DF) controller as,

$$\begin{aligned} e(t) &= F_\mathrm{ref} - F_\mathrm{e} \\ F_\mathrm{fb} &= P_\mathrm{DF}\, e(t) + I_\mathrm{DF} \int_0^t e(t)\,\mathrm{d}t \end{aligned} \tag{4}$$

where F_e is the measured angle, F_fb the desired force from the motor, P_DF the gain for proportional control and I_DF the gain for integral control. The gains govern behaviors of the controller. Therefore they were tuned for the controller to generate quick and minimum-jerky movements.

In addition, a feed-forward term of F_ref was added to F_fb in order to increase bandwidth of the controller. Thus, the final desired force from the motor can be written as,

$$F_\mathrm{DF} = P_\mathrm{DF}\, e(t) + I_\mathrm{DF} \int_0^t e(t)\,\mathrm{d}t + F_\mathrm{ref}. \tag{5}$$

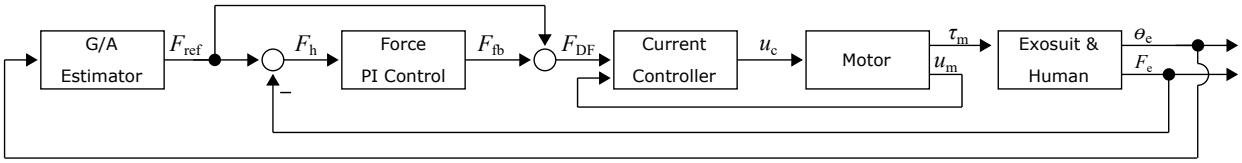

(a) Closed-loop direct force controller with a gravity-assistance feed forward

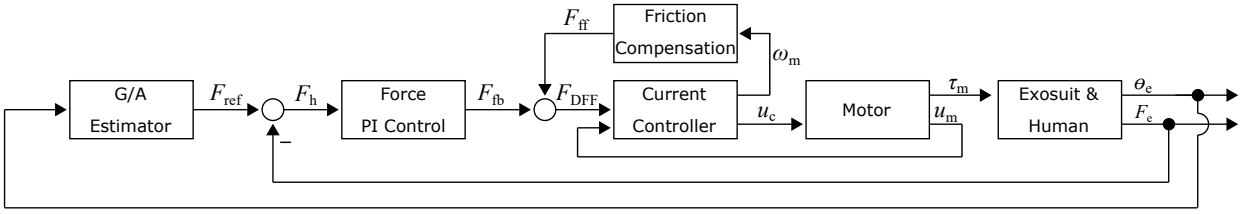

(b) Closed-loop direct force controller with friction compensation

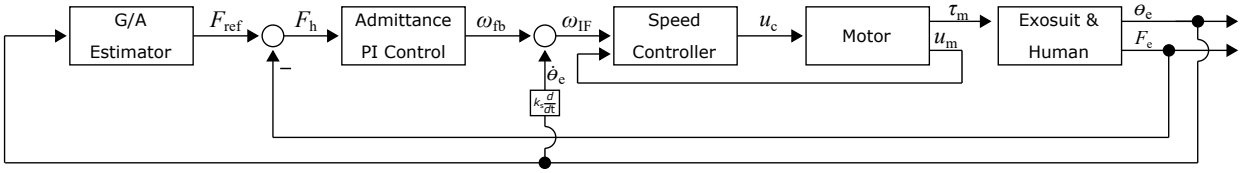

(c) Closed-loop indirect force controller

Fig. 4. Three different controllers for gravity compensation of the upper extremity exosuit. The G/A estimator estimates the required force at the end effector based on the current elevation angle. (F_{ref}: the estimated required cable pulling force for gravity compensation, F_{e}: the measured force at the end effector, F_{h}: the estimated biological force (human contribution), F_{fb}: the feedback force control signal for motor control, F_{ff}: the feed-forward friction compensation, F_{DF}: the desired force from the motor, F_{DFF}: the desired force from the motor, ω_{DF}: the desired speed of the motor, u_{c}: the control signal from the motor controller to the motor, u_{m}: the signal from the motor to the motor controller for its closed loop, τ_{m}: the torque applied from the motor to the wearer, θ_{e}: the measured elevation angle, $\dot{\theta}_{\text{e}}$: the arm elevation angular velocity, ω_{fb}: the feedback speed control signal for motor control, ω_{m}: the velocity of the motor in revolutions per minute.)

Then, the motor controller controls current to the motor to generate F_{DF} along the cable.

2) Closed-loop Direct Force Controller with Friction Compensation: On top of the direct force controller described above, a friction compensation model was added as shown in Fig.4(b). Instead of F_{fb}, the friction compensation model was implemented as a feed-forward model. The friction model includes static friction and viscous friction. Static friction depends on a normal force between the cable and the cable sheath and on their material properties while viscous friction is a function of the relative velocity between the two components. Each friction term was empirically identified as described in Appendix B and given as,

$$F_{\text{ff}}(\dot{l}) = \begin{cases} 20\,\text{N}, & \text{if } \dot{l} \leq 0.01\,\text{m/s} \\ 54.71\,\text{kg/s}\;\dot{l} + 10.59\,\text{N}, & \text{otherwise} \end{cases} \tag{6}$$

where F_{ff} is a compensating force for friction and $\dot{l}$ is a cable pulling speed. The cable pulling speed was estimated using the velocity of the motor. The desired force from the motor, F_{DFF} is then equal to

$$F_{\text{DFF}} = P_{\text{DFF}}\, e(t) + I_{\text{DFF}} \int_0^t e(t)\,\text{d}t + F_{\text{ff}}(\dot{l}). \tag{7}$$

However, the normal force is proportional to the cable tension therefore the normal force varies with different elevation angles. As a result of the varying normal force, static friction will vary as well. Also, the viscous friction can change with respect to the length of the cable and the curvature of the cable sheath [33]. More sophisticated models, namely a nonlinear friction model, have been implemented in order to capture the behavior of the friction [6], [34]. However, sophisticated friction compensation models may still be prone to changes in the cable and the sheath. For actual applications of exosuits, the length and the curvature of the cable and the sheath will differ from one user to another and it necessitates changes in the parameters of the friction model. Therefore, effort to acquire sophisticated friction models may not exceed outcome from the models. Thus, as an initial investigation, the simple friction model defined in (6) is used for the controller.

3) Closed-loop Indirect Force Controller: Unlike the other two controllers, this controller controls speed of the motor in order to indirectly control the force at the end-effector therefore is an admittance controller. Irrespective of the friction between the cable and the cable sheath, the motor will rotate corresponding to a given control signal. As long as the speed controller (see Fig.4) is tuned to be very stiff, a friction compensation model is not required because friction is accounted for by the high controller gains. Thus, the control loop can be simpler than the other two controllers.

The required force F_{ref} from (2) and the measured force F_{e} have the same moment arm of $b\,\sin(\rho)$ as shown in Fig.2. Thus, the difference in torque generated by the two forces is

$$\tau_{\text{ref}} - \tau_{\text{e}} = b\,\sin(\rho)\,(F_{\text{ref}} - F_{\text{e}}). \tag{8}$$

The difference in torque can given a function of a required

speed of the motor in the Laplace domain as

$$H(s) = \frac{\omega_{\mathrm{fb}}}{\tau_{\mathrm{ref}} - \tau_{\mathrm{e}}} = K_{\mathrm{P}} + K_{\mathrm{I}} s^{-}1 \tag{9}$$

where ω_{fb} is a desired motor speed, and K_{P} and $K_{\mathrm{I}}s$ are gains that determine the relation between the torque difference and the desired speed. Assuming the moment arm as a constant, the above equation can be expressed in terms of forces in the time domain as

$$\omega_{\mathrm{fb}} = P_{\mathrm{IF}} \left(F_{\mathrm{ref}} - F_{\mathrm{e}}\right) + I_{\mathrm{IF}} \int_0^t \left(F_{\mathrm{ref}} - F_{\mathrm{e}}\right) \mathrm{d}t. \tag{10}$$

where P_{IF} and I_{IF} are controller gains that govern the behavior of the controller.

Additionally, a positive feed-forward signal was added to ω_{fb} in order to increase transparency as well as the bandwidth of the actuation system [35]. The feed-forward term is proportional to a arm elevation speed. In other words, the motor will pull or loosen the cable faster to comply with the direction of the arm elevation movement. Consequently, the final desired speed of a motor ω_{IF} is equal to

$$\begin{aligned} e(t) &= F_{\mathrm{ref}} - F_{\mathrm{e}} \\ \omega_{\mathrm{IF}} &= P_{\mathrm{IF}}\, e(t) + I_{\mathrm{IF}} \int_0^t e(t)\, \mathrm{d}t + K_{\mathrm{s}} \dot{\theta}_{\mathrm{e}} \end{aligned} \tag{11}$$

where K_{s} is a control gain for the speed feed-forward and $\dot{\theta}_{\mathrm{e}}$ is the arm elevation speed.

D. Controller Evaluation on Test Bench

In the first experiment on the test bench, the cable was tethered to a fixed point. Instead of F_{ref} in Fig. 4, a desired force reference was used in this experiment. Properties of each controller were examined using three different inputs and its corresponding responses.

First, a step reference with various amplitudes was applied to investigate rise time, settling time and overshoot of each controller. One cycle consists of 10 different amplitudes (from 15 N to 150 N with 15 N increment) as shown in Fig. 6(a) and each cycle was repeated 4 times then averaged over repetitions. The maximum force amplitude was chosen to be $150\,\mathrm{N}$ to cover broader types of users while the required force for gravity compensation was estimated to be $120\,\mathrm{N}$ based on (2) and anthropometric data. The input reference force, F_{d}, was given as,

$$F_{\mathrm{d}} = M(t) \tag{12}$$

where $M(t)$ is the force amplitude at a given time. One amplitude lasted $4\,\mathrm{s}$ and another $4\,\mathrm{s}$ of resting time was given between one amplitude to another. During the resting time, 5 N of pretension was set in order to prevent slack along the cable.

A ramp reference from 0 to $150\,\mathrm{N}$ over $3\,\mathrm{s}$ was used to evaluate the force tracking accuracy of each controller. The force reference was repeated 4 times and the measured force was averaged over the repetitions. The input reference force was given as,

$$F_{\mathrm{d}} = k\,t \tag{13}$$

where k is the slope of the ramp, 50 N/s.

Lastly, a sinusoidal signal was used to verify the bandwidth of each controller. Duration of each frequency varied from $60\,\mathrm{s}$ to $20\,\mathrm{s}$ for the slow to the fast movements. The first $5\,\mathrm{s}$ of the obtained data was excluded for analysis assuming that the system took $5\,\mathrm{s}$ to account for settling time. The frequency band was chosen based on the requirements in ADLs, ranging from 0.05 to 2.5 Hz.

$$F_{\mathrm{d}} = \frac{1}{2} F_0 \left(\sin(2\pi f t - \frac{\pi}{2}) + 1\right) \tag{14}$$

where F_0 is 150 N and f is a frequency at a given time.

Another experiment was performed using the test bench with a pendulum. The cable was tethered to the pendulum instead of the fixed point as shown in Fig. 2. All three controllers shown in Fig. 4 were tested with the pendulum. Unlike the fixed point test, a desired reference was not fed to the controller. Instead, the pendulum was manually manipulated by a hand following an elevation angle trajectory shown on a screen as a visual angle reference. The measured angle from the IMU was shown on the same screen as visual feedback and was used for control. The angle trajectory consisted of three different amplitudes (30°, 60° and 90°) and each amplitude was repeated 4 times.

E. Controller Evaluation on Exosuit

Exosuits have inherently compliant structures. Therefore, the human, providing stability, is an integral part of the whole system. To technically evaluate feasibility and performance of the developed controllers on the exosuit, measurements involving humans are essential. Also, before any further study using the device with impaired or weak individuals, the device must be tested with able-bodied individuals as a pilot study with a tentative experiment procedure for the main study. Since it was a pilot test for technical evaluation of the controllers on the exosuit on an able-bodied human, a waiver for the ethics was acquired. Four participants (2 males, 2 females, age: $25.8 \pm 3.9\,\mathrm{years}$, height: $171.5 \pm 8.5\,\mathrm{cm}$, weight: 65.3 ± 3.9), who did not present any evidence and known history of skeletal or neurological diseases and exhibiting intact joint range of motion and muscle strength, within the same research group were recruited for small-scale pilot tests. Informed consent and participation agreement were provided to the participants. Thus, they were aware of that the experiment is conducted for a prototype test and technical evaluation of the developed controllers and the exosuit. Also, the participants were verbally informed and instructed again before and during the experiment.

According to the performance test results on the test bench, the DF controller (direct force controller with a gravity assistance feed-forward) and the IF controller (indirect force controller) were chosen for technical evaluation on the exosuit with human participants.

The experimental setup is illustrated in Fig. 5. The participants wore the exosuit with all the electric components and the actuation system connected while the motor was still mounted on the test bench. Each participant was instructed to lift and lower his/her arm according to reference angle trajectories

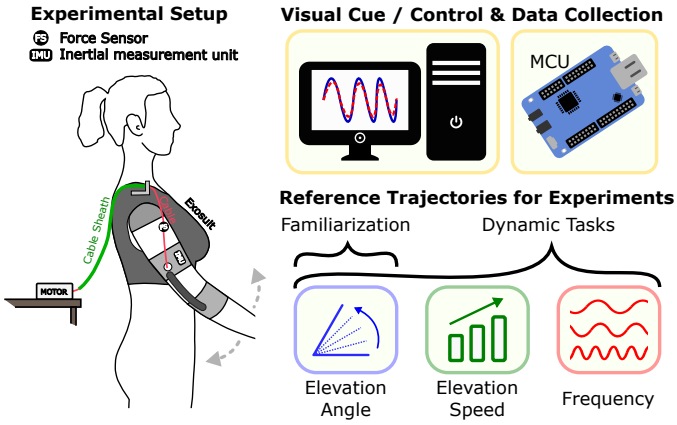

Fig. 5. Experimental setup for a small-scale, group-internal pilot test with human participants. Participants were wearing the exosuit with the upper arm and lower arm cuffs. The angle trajectories were shown on a monitor and data was collected using a microcontroller unit (MCU).

shown on a monitor. The measured arm elevation angle was also shown on the same monitor for visual feedback.

The experiments consisted of familiarization and two dynamic tasks. All experiments were conducted with the exosuit on. Three different conditions were applied, namely with no controller on (unpowered) and with each controller on (powered). When unpowered, the cable to the upper arm cuff was untethered from the actuator so as to remove possible influence or interference of the cable on participant's movements. As the aim of the Myoshirt is to provide a supplementary assistance to users who can still perform ADLs, the exosuit is not always required to provide full assistance for gravity compensation. Thus, seventy-five percent assistance, meaning $75\,\%$ of the required force for gravity compensation, was provided during the pilot test on the exosuit.

Familiarization was performed in order for the participants to get used to experimental protocol and assisted movements with the actuation system. During the procedure, the G/A estimator was validated using a simple position controller demonstrated in Appendix A. The participants were asked to remain passive while the controller sent commands out to the motor to move the participant's upper arm from $0°$ to $90°$ and repeated the movements three times. The measured force was compared with the estimated force using the G/A estimator with respect to the elevation angle. Then the estimator was tuned accordingly.

In order for the participants to get accustomed to the device, they were asked to follow a minimum jerk trajectory (MJT) on the screen. The trajectory is a 5th order polynomial consisting of three different elevation angles ($30°$, $60°$, $90°$) but with the same peak elevation speed of $84\,°\,\mathrm{s}^{-1}$, which was fifty percent of the peak elevation speed during the fast arm elevation derived from (3). The order of elevation angles was randomized and each angle was repeated 4 times during the test as illustrated in Fig.8(a).

To evaluate the performance of the controllers, two different dynamic tasks were conducted.

For the first dynamic task, the same MJT during the familiarization was used again. The participants could project the trajectory two seconds ahead on a monitor. As outcome measures, the arm elevation angle measured with the IMU and interaction force measured with the force sensor were collected.

For the second task, a sinusoidal trajectory with different frequencies, corresponding to different peak arm elevation velocities as derived in (3), was tested in order to define bandwidth of each controller. The reference angle trajectory was given as,

$$\theta_{\text{ref}} = 50° + 40°\sin(2\pi f(t)t) \tag{15}$$

where $f(t)$ is a given frequency for each test that corresponds to one peak elevation speed. The participants started with their arm elevated to $50°$, then moved their arm within $10°$ to $90°$ following the trajectory shown on the monitor. The frequency ranged from 0.05 to $1\,\mathrm{Hz}$ with increments of $0.05\,\mathrm{Hz}$. Each trajectory lasted from 20 to $60\,\mathrm{s}$. The arm elevation angle and the force were measured during the task but the first few cycles of the measured data were not taken into account for data analysis with assumption that humans would take a few seconds to reach steady state after a few cycles.

All the tests were conducted on the same day with a 5 minutes break between each condition.

F. Data Analysis

All the required data for analysis such as the elevation angle and the assistive force were collected using the microprocessor with a sampling frequency of $200\,\mathrm{Hz}$. The collected data was low-pass filtered with the second order Butterworth filter with $10\,\mathrm{Hz}$ cut-off frequency before analysis.

For the experiment on the test bench with the fixed point, the rise time, settling time and overshoot were defined for each controller based on the step response. Additionally, the accuracy of force tracking for each controller was obtained from the results of the ramp response. The root mean square error (RMSE) was used to quantify the accuracy performance of the controllers as,

$$\text{RMSE} = \sqrt{\frac{1}{n}\sum_{t=t_0}^{T} e_t^2} \tag{16}$$

where e_t is the error between the reference and measured signals and n is the number of data points between the time t_0 to T. For the sinusoidal trajectories, a Bode plot was used to acquire the force bandwidth of the controllers. The half-power point bandwidth definition, where the amplitude drops by 3 dB of its low frequency asymptotic, was used to determine bandwidth of controllers.

For the test bench with the pendulum, the RMSE in the elevation angle was calculated between the reference and measured data to analyze the tracking accuracy over given conditions. Also, the estimated force and the actual measured force were compared in order to verify if a lifting motion was assisted during the task. The difference of the two forces can be interpreted as the external force applied to the pendulum and therefore, can be considered as human contribution to move and hold the pendulum. Therefore, it can validate whether the lifting motion was assisted.

The tracking accuracy of the controllers from the first dynamic task on the exosuit was quantified using RMSE by comparing the reference arm elevation angle to the measured angle. The reference force and the measured force were also compared with the same metric. The data was also analyzed with respect to different elevation angles to check whether the controllers perform differently. Not only the RMSE, the smoothness of the movement was also evaluated with the SPectral ARC length (SPARC) index to quantify whether the actuation system interferes with the user's natural movements [36]. The lower magnitude of the SPARC indicates smoother movements.

For the second dynamic task, the Fourier coefficients of the reference and measured angles of each tested frequency were calculated and the Bode plot was drawn. Because the reference force, derived in (2), does not have a linear relationship with the elevation angle, the reference force consists of multi-sinusoidal signals with respect to a sinusoidal angle reference. However, since the movement was periodic with one frequency at a time, the major frequency of the reference force had the same major frequency as the movements. Thus, in order to determine the force bandwidth, a Fourier coefficient of one major frequency of each movement speed was analyzed.

The difference or error between the reference force and the measured force can be interpreted as human contribution to hold the arm at an instant elevation angle. The force error demonstrates that the controllers were not able to provide corresponding assistance when the value is negative and the controllers provided more force than required when the value is positive. The normalized mean force error, F_{ne}, over different frequencies can therefore identify whether the controller is capable of providing adequate assistance to a user with respect to arm movement frequencies. The metric is given as,

$$F_{\mathrm{ne}} = \frac{1}{n}\sum_{t=t_0}^{T}\frac{F_{\mathrm{m}} - F_{\mathrm{ref}}}{F_{\mathrm{ref,max}}} \tag{17}$$

where F_{m} is the measured force, F_{ref} is the reference force, $F_{\mathrm{ref,max}}$ is the maximum reference force and n is the total number of samples for each analyzed frequency between the time t_0 to T. The negative force error and the positive counterpart were integrated individually as the two values cancel each other out and indicate different behaviors between the user and the device. In addition, the time lag between the reference force and the measured force was obtained where the cross-correlation between the two forces was the highest in order to validate if the controllers apply force at the right timing with the right corresponding direction of assistance.

III. Results

A. Test Bench with Fixed Point

Figure 6 shows the performance of each controller with the three different reference inputs.

For the step response shown in Fig.6(a), the IF controller showed consistent performance over various force magnitudes while the direct force controllers' performance varied from one magnitude to another.

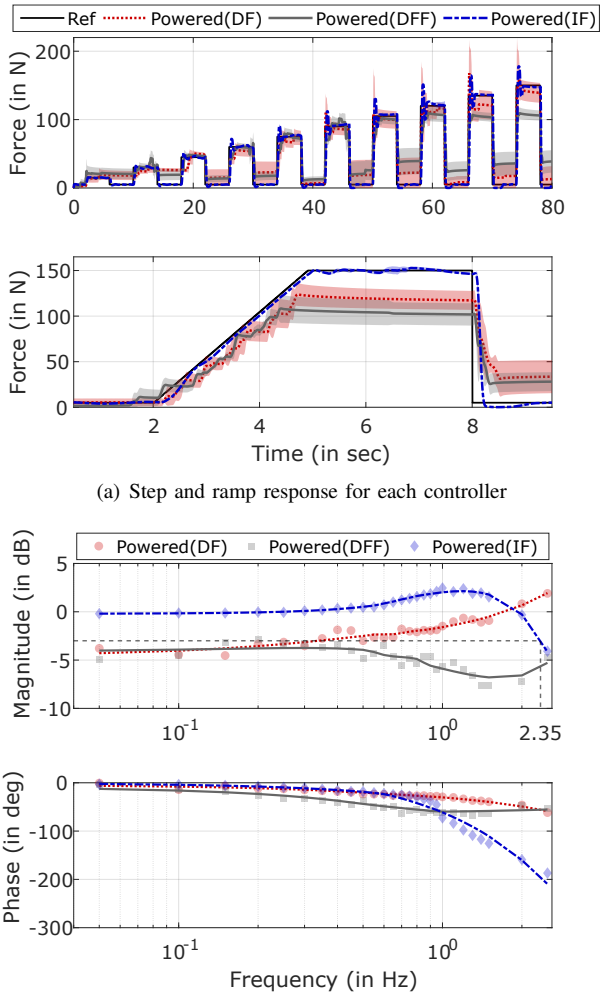

(a) Step and ramp response for each controller

(b) Bode plot for each controller

Fig. 6. Performance test results on the test bench with a cabled tethered to a fixed point. (a) The shaded area shows the standard deviation of each controller for the corresponding colors. While the IF controller showed very consistent behavior, the other direct force controller's performance varied a lot over repetitions. (b) The mean curves of each condition were fitted using the Savitzky-Golay filter. The IF controller showed the bandwidth of 2.35 Hz. The bandwidth of the two controllers cannot be identified within the tested frequency range because the magnitude of the other two controllers did not drop by 3 dB from the initial magnitude at the low frequency.

The Powered(IF) condition showed an average overshoot of $18.6 \pm 7.5\,\%$ throughout the different force magnitudes. For both of the direct force controllers, not only overshoot but undershoot occurred as well. The rise time for the Powered(IF) was $0.27 \pm 0.02\,\mathrm{s}$ while the Powered(DF) showed $0.63 \pm 0.79\,\mathrm{s}$. The DFF controller could not reach the $90\,\%$ of the desired force for the two highest force amplitudes. Excluding the two data points, the rise time for the DFF controller was $0.71 \pm 0.35\,\mathrm{s}$. The settling time was also obtained over the three conditions and the IF controller took $0.68 \pm 0.34\,\mathrm{s}$ to settle. However, the other two direct force controllers did not reach the equilibrium values of the settling time for almost half of the different force amplitudes. Except the data where the direct force controllers could not remain within specific error band for the settling time, the settling time was obtained $1.59 \pm 1.19\,\mathrm{s}$ and $1.44 \pm 1.41\,\mathrm{s}$ for the Powered(DF) and

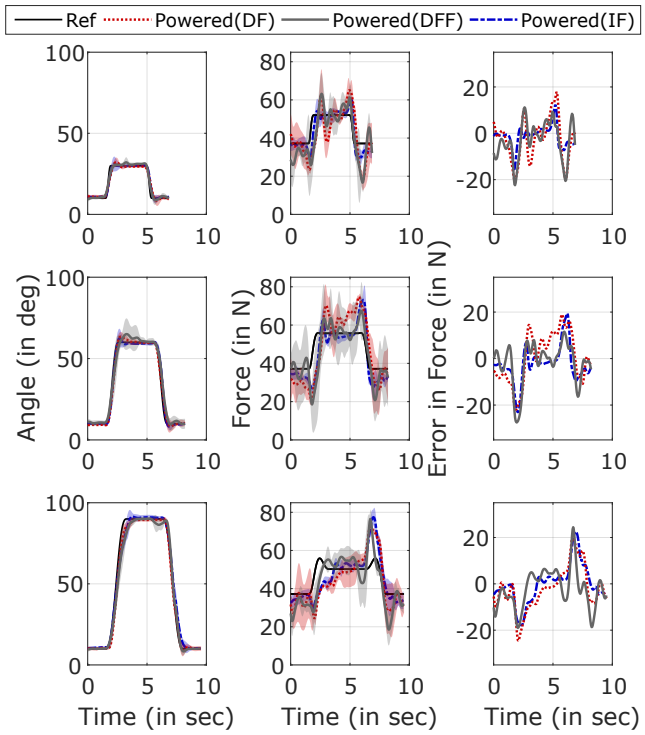

Fig. 7. Angle Tracking Test Result on the test bench with a pendulum. The tested result was investigated in terms of each elevation angle. The shaded area shows the standard deviation of each controller for the corresponding colors.

Powered(DFF) conditions, respectively. Regarding the ramp response shown in Fig.6(a) (bottom), the IF controller showed the best accuracy with the RMSE of 17.12 N while the DF controller (RMSE of 27.61 N) and the DFF controller (RMSE of 32.75 N) performed much worse. The direct force controllers could not reach the desired force, resulting in a considerably high force error. In addition, the performance of force tracking varied a lot for the direct force controllers as the DF controller and DFF controller had standard deviation (SD) 2.5 times greater than the IF controller. The average SD of the IF controller was 0.99 N while the DF and DFF controllers had 10.95 N and 9.38 N, respectively.

Figure 6(b) shows the controller's behavior over the tested frequency range. The force bandwidth of the IF controller is approximately 2.35 Hz while we could not identify the bandwidth of the two direct force controllers because the magnitude for both controllers did not drop by 3 dB within the tested range.

B. Test Bench with Pendulum

The RMSE in the elevation angle showed $4.82°$, $4.29°$ and $5.79°$ for the Powered(IF), Powered(DF) and Powered(DFF) conditions, respectively. The RMSE in force was 9.08 N, 12.81 N and 14.79 N for the three conditions, respectively as above. The IF controller and DF controller performed better than the DFF controller in terms of both angle and force tracking accuracy.

C. Exosuit

Based on the performance evaluation (force tracking, angle tracking and performance consistency) with the test bench, two controllers, the direct force controller with gravity-assistance feed forward and the indirect force controller, were chosen for the technical evaluation of controllers on the exosuit with human participants in our pilot study.

The result of MJT from one participant is shown in Fig.8. Angle tracking accuracy of the controllers was evaluated using the RMSE. Figure 9 (right) shows the RMSE in the elevation angle over all participants for the unpowered and two powered conditions. The average RMSE for each condition is $3.87 \pm 0.95\,°$, $3.95 \pm 1.00\,°$ and $3.21 \pm 0.65\,°$ for the unpowered, the DF controller and the IF controller, respectively. Similar to the RMSE, the smoothness between the conditions did not vary much. The overall smoothness in the elevation angle over the participants is -4.00 ± 0.37 for the unpowered, -4.19 ± 0.24 for the powered(DF) and -4.20 ± 0.03 for the powered(IF) condition.

The measured angle was mapped to the reference force using the G/A estimator. Then the measured force was compared with the reference force. During the unpowered condition, assistive force was not applied. Thus, only two powered conditions were compared as illustrated in Fig.10. The overall RMSE in the force is 2.95 ± 0.15 N for the IF controller and 9.34 ± 2.99 N for the DF controller. The smoothness of movements for each controller is -4.70 ± 0.61 and -7.07 ± 0.89 for the IF controller and the DF controller, respectively.

The obtained data was also investigated in terms of different elevation angles as shown in Fig.8(b). The RMSE in each elevation angle varied from $2.60°$ to $4.82°$ over the three conditions. However, the RMSE in force varied relatively a lot over different elevation angles and the conditions. The IF controller did not show considerable difference in the force RMSE varying from 2.80 N to 3.22 N. However, the force RMSE for the DF controller showed 12.67 N, 7.34 N and 7.50 N for $30°$, $60°$ and $90°$ of the elevation angles, respectively.

From the second dynamic task, a Bode plot with respect to each tested movement frequency for the two powered conditions was obtained as shown in Fig.11. The participants were able to track the reference movements without a noticeable delay or reduction in magnitude of the motion within the given frequency range. Thus, the position bandwidth of the controllers is greater than 1 Hz which is above the target bandwidth of 0.67 Hz.

Despite the fact that the participants were able to follow the angle trajectory of 1 Hz, the force showed considerably different results to the position. As shown in Fig.12, the force magnitude increased with an increasing moving frequency and also the phase shift turned more salient for both tested controllers. Within the tested frequency range and based on the half-power point bandwidth, the bandwidth could not be identified as the force magnitude for both controllers did not show reduction in magnitude of 3 dB. Increase in the magnitude can indicate that the controllers hinder user's movements

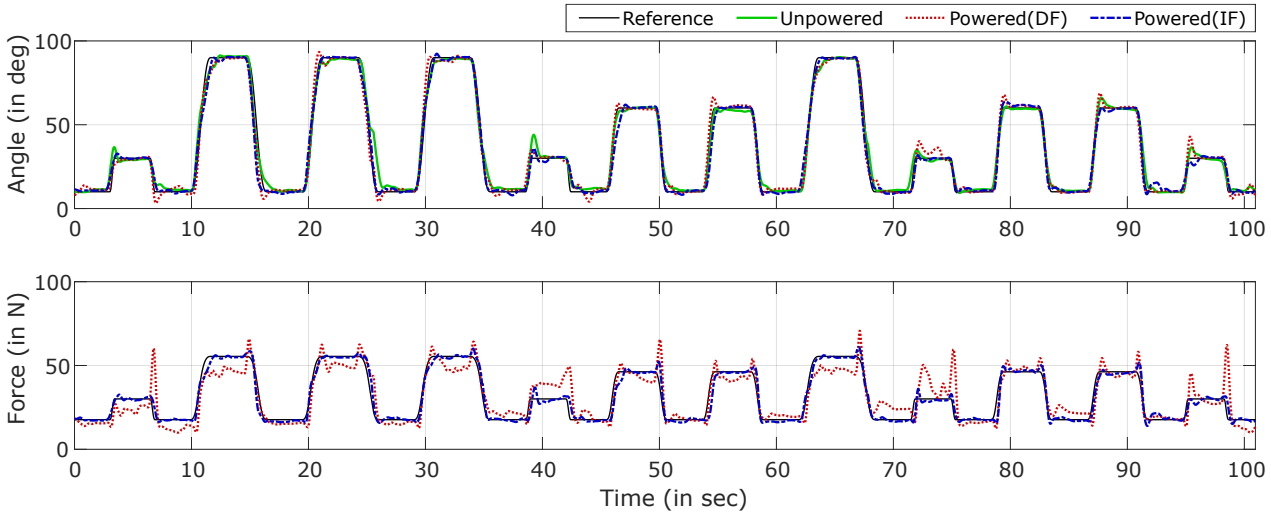

(a) Tracking accuracy for the minimum jerk trajectory in the elevation angle and the corresponding force from one participant

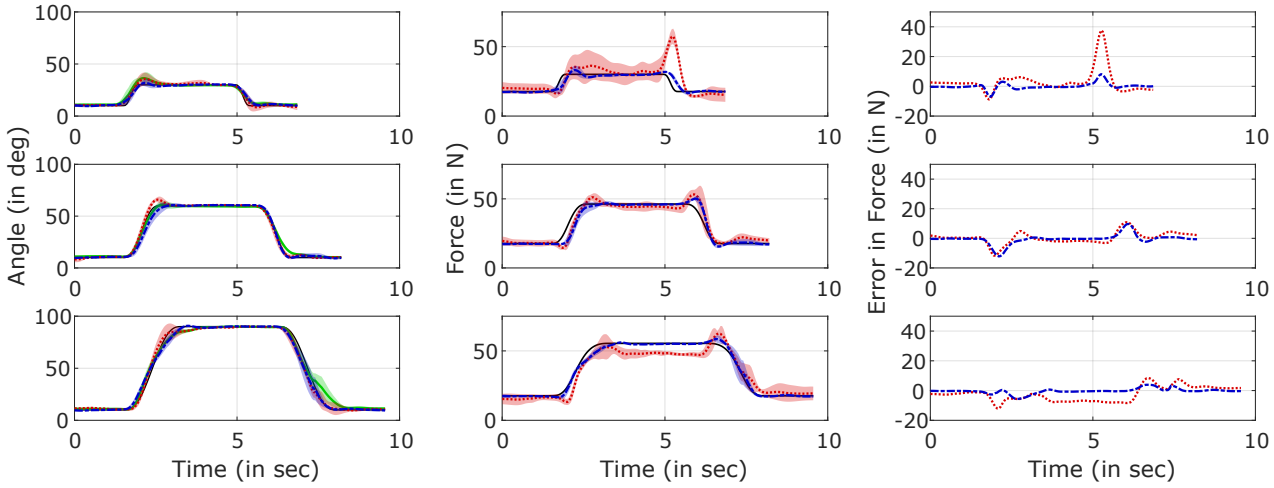

(b) Tracking accuracy for three different elevation angles of 30°, 60° and 90° from the same participant above

Fig. 8. (a) Three different conditions were tested for the with the peak elevation velocity of $84\,^\circ\,\mathrm{s}^{-1}$. The three conditions consisted of unpowered, powered with direct force control (DF) with a positive gravity-assistance feed forward and powered with indirect force control (IF). The root mean square error(RMSE) in the elevation angle is 3.48°, 3.44° and 3.53° for unpowered, powered(DF) and powered(IF) conditions, respectively. The RSME in force is 2.93 N and 7.18 N for the powered(DF) and the powered(IF) conditions. (b) The shaded area indicates the standard deviation in the corresponding conditions for each color. The measured force dropped when arm elevation initiated and jumped when arm demotion initiated regardless of the conditions. The powered(DF) condition showed greater dips and peaks.

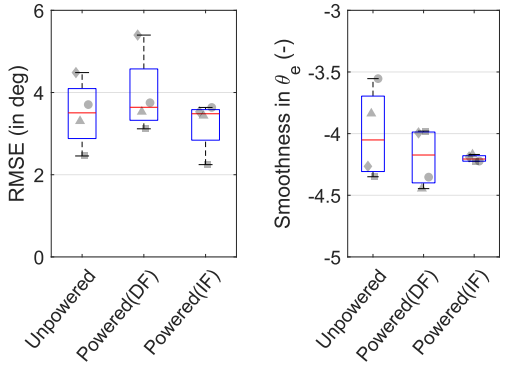

Fig. 9. The RMSE and smoothness of movement in the elevation angle during the MJT tracking task over all participants.

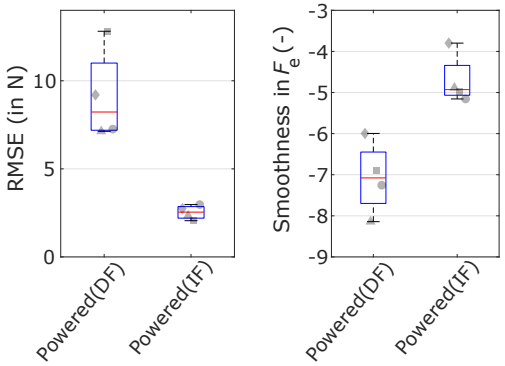

Fig. 10. The RMSE and smoothness of movement in the assistive force during the MJT tracking task over all participants.

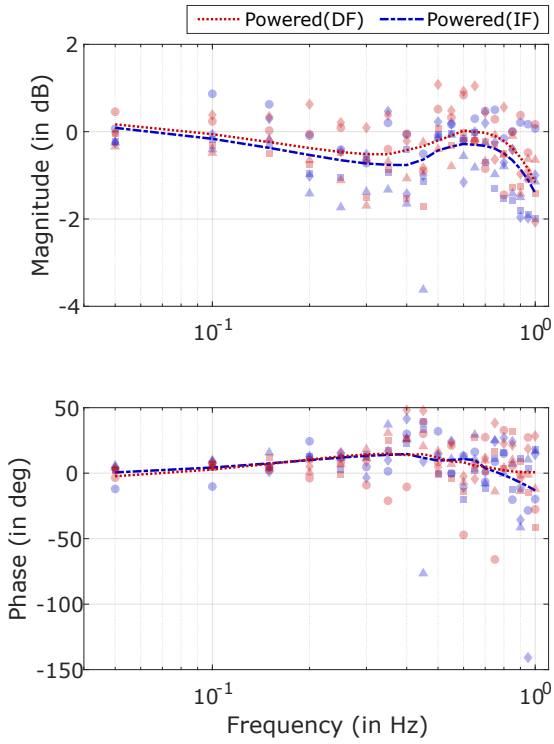

Fig. 11. Position Bode plot for the two powered conditions. The mean curves were fitted using the Savitzky-Golay filter. Each symbol represents one participant and the color indicates each condition. The participants were able to track the reference movements up to 1 Hz without a considerable phase delay or reduction in magnitude.

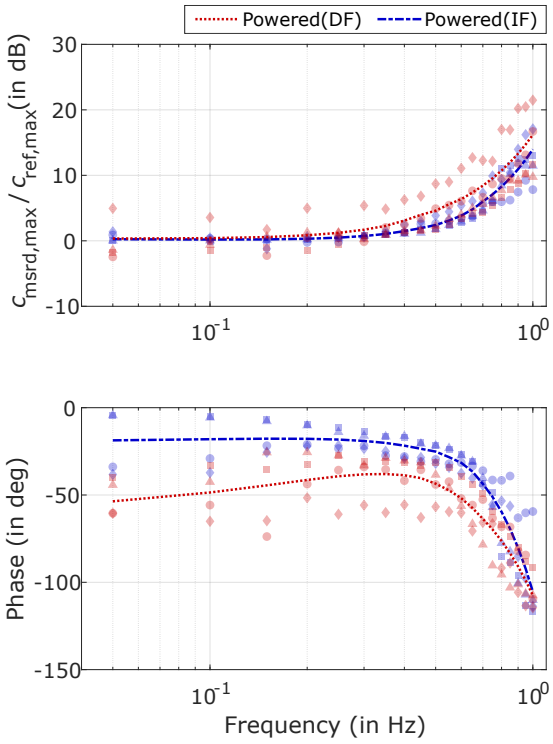

Fig. 12. Th coefficient ratio and phase difference between the reference and the measured forces. The mean curves were fitted using the Savitzky-Golay filter. The magnitude of force increased with increasing moving frequencies while the phase difference worsened with the higher frequency. Thus, the actuation system applied more force than was required with substantial phase shift to the participants, therefore the systems could have hindered the participant's movements.

because the users receive more force than needed for gravity compensation therefore can indicate poor performance of the controllers as well. Thus, instead of -3 dB, the bandwidth was defined at a frequency where 3 dB increment in magnitude occurs. Accordingly, the IF controller had 0.55 Hz and the DF controller 0.4 Hz.

Similarly, the magnitude of the force error between the reference and measured force also increased with the increasing movement frequency as shown in Fig.13. The normalized mean force errors were investigated separately for negative and the positive values. The overall negative force error for both controllers decreased from -3.32 % to -35.61 % for the IF controller and from -5.76 % to -34.74 % for the DF controller. The overall positive force error also increased from 2.66 % to 55.2 % and from 10.84 % to 82.28 % for the IF and DF controllers, respectively. The time lag between the reference force and the measured force got worse over the increasing frequency. Especially from 0.5 Hz, the time lag for the both controllers dropped below -0.14 s for the IF controller and -0.22 s for the DF controller. This similarly follows the result of the force bandwidth of each controller.

IV. Discussion

The aim of this pilot study was to evaluate the feasibility and performance of different controller frameworks in order to find a more suitable solution for the shoulder exosuit. Also, based on the results and observations during the experiments, we suggest some improvements in the controllers and the experiment procedure for the main study and the future work.

A. Performance Comparison

The indirect force (IF) controller outperformed the other two direct force (DF, DFF) controllers on both the test bench and the exosuit.

1) Test Bench: From the obtained result on the test bench, the IF controller showed consistent performance over different tasks while the other two controllers' performance showed significant variance within and over each task.

The two direct force controllers could not reach the maximum reference force even when the motor was on full power. That is because the applied force at the fixed point is not equal to the generated motor force because of force losses during transmission. The problem could have been solved if the controllers were tuned more stiff, meaning higher controller's gains. However, when the gains are high, it can result in significant overshoot and jerky movements which are not desired for the exosuit.

In addition, for the direct force controllers, the motor can only apply the pulling force meaning that the motor does not rotate in the direction to slack the cable unless it is pulled by an external force. Thus, when force drops from high to low, the motor shaft is only pulled by the recovering force of the cable

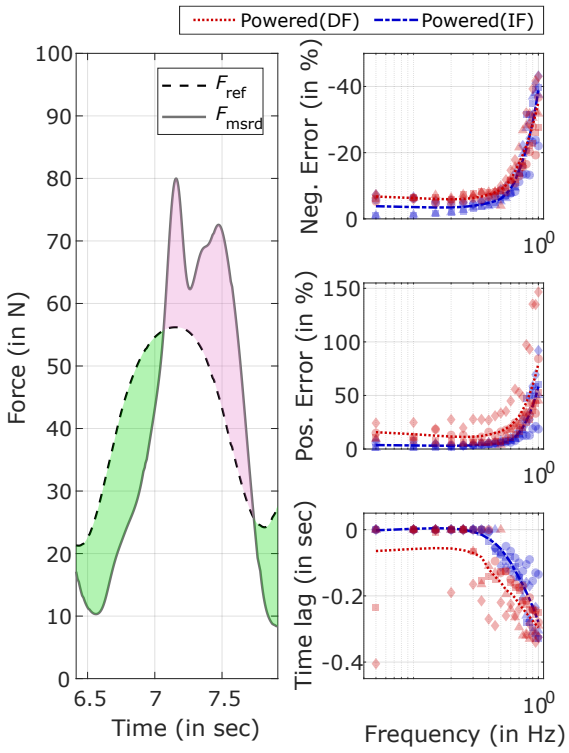

Fig. 13. Normalized mean force errors between the reference force, F_{ref}, and the measured force, F_{msrd}. The mean curves for the errors and time lag were fitted using the Savitzky-Golay filter. The magnitude of the normalized negative error (green-shaded area) increases with increasing movement frequencies. Also, the positive error (pink-shaded area) increases with the increasing movements. The higher the movement frequency is, the worse the time lag is. Both negative error and positive error show more dramatic change as soon as a time delay is substantial.

which reduces the cable tension. However, the recovering force sometimes may not be sufficient to overcome friction resulting in the remaining cable tension. Thus, it leads to a considerable force error during the pretension phase. Nevertheless, with the exosuit on a human, the cable will be pulled by the weight of his/her arm. Therefore, this phenomenon is not expected to occur with the exosuit.

The result on the test bench with the pendulum showed similar tracking performance both in the angle and the force for all three controllers regardless different elevation angles. The measured force fluctuated to some extent because the weight added to the pendulum swung during the test leading to varying the force. This again does not occur with the exosuit.

Based on the performance evaluation, the IF controller and the DF controller were selected for the pilot test on the exosuit and are recommended to use for the main study as well. Another reason for the DFF controller not being selected was the friction model. The friction force is cumbersome to be modeled because its properties change with curvature and length of the cable and the cable sheath [33], [37]. Thus, when it comes to an actual application, the model will not be very robust and transferable from one user to another.

2) Exosuit: Two dynamic tasks (MJT, sinusoidal responses) were conducted for each controller on the exosuit. The IF controller showed better performance than the DF controller in both tasks.

In the first dynamic task, the performance of angle and force tracking was evaluated. The IF controller showed better performance in the tracking accuracy and smoothness of the movements. Both DF and IF controllers did not show significant difference from the unpowered condition regarding the position tracking task with MJT. This can be interpreted as the controllers did not interfere with the natural movements of the users. However, the DF controller showed worse force tracking performance. This could be a result of the motor not moving at all during the low elevation movement ($30°$). That is assumed to occur because the tensile force is not sufficient to overcome the static friction force which also was observed with the test bench. Smoothness was also worse for the DF controller. During the task, some jerk movements were observed during elevation and demotion of the upper arm over all participants. In addition, the force drop and jump were observed right before the elevation and demotion of the upper arm initiated as shown in Fig.8(b) (right). This behavior occurs because the cable either slacks or is pulled when the participants initiate movements. Nevertheless, both controllers could manage to remove slack and over-tension on the cable as the force error converged to 0 quickly.

In the second dynamic task on the eoxsuit, both angle bandwidth and force bandwidth were obtained. Based on the half-power point bandwidth definition, both controllers had over 1 Hz position bandwidth which is higher than the targeted bandwidth of 0.67 Hz. However, the force bandwidth of the controllers was lower than 0.67 Hz. Moreover, the phase in force dropped below $-100°$. As a result of high phase difference, the assistive force is delivered with substantial delay therefore starts hindering the user's movements, leading to exacerbating transparency of the device.

A similar tendency is observed in the force error shown in Fig.13. As soon as the time lag becomes more salient above 0.55 Hz, both negative and positive force errors become considerably worse. This describes that with faster arm elevation movements, the controllers cannot exert an assistive force at the right moment which hinders user's movements consequently. Thus, the time lag can also be used as a performance measure for the transparency of the exosuit in the future studies. From the study in the influence of delay between a prosthesis device and the user [38], the acceptable delay of the device was reported to be below 150 ms in order for the users to recognize the device the least. However, exosuits are an orthosis device therefore the acceptable delay of 150 ms may not be applicable but it can still provide an idea of the transparency of orthosis devices. Accordingly, the time lag dropped below 150 ms after 0.45 Hz for the DF controller and 0.6 Hz for the IF controller. The frequencies for the time lag similarly follows the obtained force bandwidth of each controller.

B. Suggestions from Pilot Study

According to the test results and the performance evaluations on the exosuit in our pilot study, the indirect force controller showed better performance than the direct force

controller. Despite some promising results of the IF controller, there were several limitations in the pilot study which suggest some improvements for the main study and future work.

First of all, the controller's performance can be improved. Both IF and DF controllers could not reach the targeted force bandwidth of 0.67 Hz. Including a stiffness model of an exosuit can improve the bandwidth of controllers [39], [40]. A small experiment will be required to establish the stiffness model. As long as the same exosuit is in use for the experiment, the model can be transferable for different participants unlike the friction model. Also for the future work, sensor fusion of the IMU and the motor encoder can better estimate the arm elevation angle. Consequently, the tracking performance can be improved.

The exosuit showed severe deformation during the tasks. The displacement of the cable guide (see Fig.2) has a significant influence on the G/A estimator due to the exosuit's geometry. Additionally, the same cable guide was used during the experiments as an initial investigation, therefore it did not fit every participant. For the main study, cable guides with various sizes for participants may help conclude to better performance of the exosuit.

For technical evaluation of controllers, RMSE and smoothness of assistive force and arm elevation angles were related to influence of the controllers on the natural movements of users because they are likely to be affected by user's movements. Nevertheless, the two evaluation terms may not suffice to validate whether the user's natural movements are not invaded by the controllers. It will be beneficial for the main study to have a better validation approach such as a 3D motion capture system. Additionally with the current experiment setup, the measured angle can only show an elevation angle thus cannot detect any compensatory/unnatural movements of participants following a trajectory shown on a monitor.

During the technical evaluation, the negative and the positive force errors were used as a parameter to determine if the controllers were able to provide sufficient assistance with respect to different movement frequencies. However, those errors do not provide a concrete evidence of assistance because there can be some model discrepancy in the G/A estimator and also they do not directly show if the movements are assisted. Thus, in the main study, measuring muscle activities such as EMG during experiments is recommended to get more robust evidence of assistance provided to a user from the actuation system.

The current experiment procedure may not be sufficient to validate that the controller's capability for assistance as the participants were instructed to follow simple trajectories in the saggital plane which do not reflect general activities of daily living. Some tasks involving ADLs can be introduced in the experiment procedure of the main study. It can also indicate whether the requirements of the controllers were set higher or lower than were needed. However, ADLs include flexion/extension of the elbow joint which changes the net required torque for gravity compensation at the shoulder joint. The current G/A estimator will not work once the elbow movements are included. Thus, another IMU needs to be implemented to measure the elbow flexion angle and the G/A estimator should also be re-defined including the elbow angle.

For the powered conditions, the participants received 75 % of assistance from the device. The performance of controllers may differ when a different assistance level is applied. Less assistive force may feel more comfortable for fast movements because there will be less force to hinder user's movements when there are severe phase shift or time lag. Also, a higher assistive level may feel more comfortable especially when the upper arm moves slowly since the assistive force can hold a user's arm therefore less human contribution for gravity compensation of the arm. For the future study, applying different assistance levels can be favorable because different user groups may prefer different assistance levels.

The G/A model, used to map the elevation angle to the required force, was obtained using a position controller for each participant. Tuning the model was done manually for each participant which can be repetitive. Because the model is assumed to include user's antropometric data, the model can be systematically studied and defined with respect to the antropometric data or other factors. Consequently, for the future work, the model identification can be automated so that the controller can be easily adapted to each individual.

V. Conclusion

Various types of controllers can be used for soft exoskeletons for assistance. In this paper, three closed-loop controllers (the direct force PI controller, the direct force PI controller with friction compensation and the indirect force PI admittance controller) were tested on a customized test bench. Because the force controller with friction compensation has its drawbacks such as difficulty to get a sophisticated model and jerky movements, the direct force PI controller and the indirect force PI controller were selected and evaluated on an upper limb soft exoskeleton. Although the analyzed results may not be sufficient to validate that the controller's ability to provide the right amount of assistance at the right time, the indirect force admittance controller shows more promising results and capability of accommodating faster arm elevation movements than the direct force controller, therefore can be used for the main study and human trials.

Acknowledgments

I would like to thank Professor Robert Riener for giving me an opportunity to work in such a fascinating lab and also to the lab members for their help. Special thanks to my supervisor, Anna-Maria Georgarakis and Michele Xiloyannis, for their technical support.

APPENDIX A
GRAVITY-ASSISTANCE MODEL VALIDATION

$$\tau_{\mathrm{g}} = \tau_{\mathrm{ref}} + \tau_{\mathrm{h}}$$
$$\tau_{\mathrm{ref}} = b\,\sin(\rho)\,F_{\mathrm{ref}}$$
$$\rho = \mathrm{acos}\left(\frac{b + a\,\cos\left(\phi+\theta\right)}{\sqrt{a^2+b^2+2\,a\,b\,\cos\left(\phi+\theta\right)}}\right)$$
$$F_{\mathrm{ref}} = \frac{\tau_{\mathrm{g}} - \tau_{\mathrm{h}}}{b\sqrt{1-\frac{(b+a\,\cos(\phi+\theta))^2}{a^2+b^2+2\,a\,b\,\cos(\phi+\theta)}}}$$

The above equation shows the relation between the gravitational torque at the shoulder joint to a required assistive force for gravity compensation.

In order to verify the model, a position controller was implemented which pulls the participant's arm to 90° over 5 s and lowers it to 10°. It was repeated 3 times but the data of the first cycle was excluded for the analysis as settling time. The result from one of the participants is shown in Fig.14.

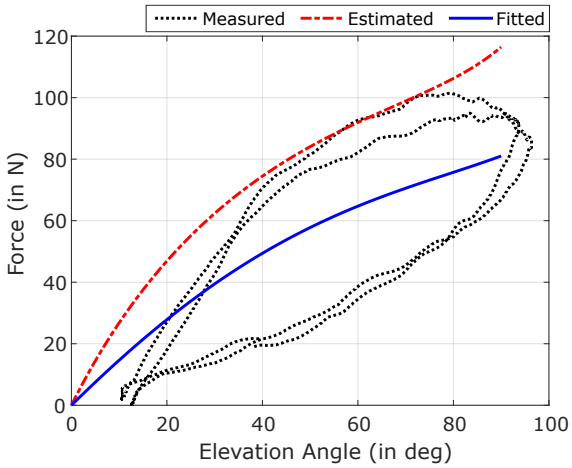

Fig. 14. Gravity-Assistance model validation. It shows hysteresis in force for arm lifting and lowering movement. The estimated model follows the upper curve but is off from the lower curve. Thus, a line was fitted using the mathematical model above.

Hysteresis in force between arm elevation and motion was observed. The estimated model followed the upper curve of the measured data. However, it showed a significant difference to the lower curve. Thus, an estimation model was obtained by using (18) and fitting a curve between the upper curve and the lower counter part. Six parameters such as a_1, b_1, b_2, c, d_1, d_2 were optimized by fitting a line between the upper/lower curves using the interior-point algorithm.

$$F_{\mathrm{ref}} = \frac{a_1 \sin(\theta)}{\sqrt{1-\frac{b_1+b_2\cos(c+\theta))^2}{d_1++d_2\cos(c+\theta)}}} \tag{18}$$

The fitted curve was obtained for each participant and used for the G/A model for the controller during the pilot test on the exosuit with human participants.

APPENDIX B
FRICTION MODEL

For cable drive with a cable sheath, it often introduces considerable friction between the cable and the sheath as shown in Fig. 15. Friction includes static friction and dynamic friction depending on a relative speed between the two components.

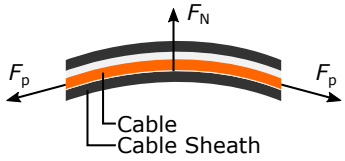

Fig. 15. Cross section diagram for a cable and a cable sheath. F_N is a normal force between the cable and the sheath and F_p is a cable pulling force.

The static friction is proportionate to the normal force between the cable and the cable sheath. Also, the normal force increases as the cable pulling force increases due to the configuration of the geometry of the exosuit.

$$\begin{aligned} F_{\mathrm{s}} &= \mu_{\mathrm{s}} F_{\mathrm{N}} \\ F_{\mathrm{N}} &\propto F_{\mathrm{p}} \end{aligned} \tag{19}$$

where F_{s} is the static friction force, μ_{s} the coefficient of static friction, F_{N} the normal force and F_{p} the cable pulling force.

The dynamic friction occurs when the cable moves relative to the cable sheath and it is a function of the cable pulling speed.

$$F_{\mathrm{d}} = f(v) \tag{20}$$

where F_{d} is the dynamic friction force and v is a relative velocity. There are several trends of the dynamic friction which are defined as stribeck friction, coulomb friction and viscous friction.

The effective cable length for the friction is constant because there is hardly any elongation of the cable sheath. Also, dramatic change in the cable sheath curvature is not expected. Thus, a simple friction model has been identified empirically.

The weight of 500 g was added at the end of the cable as shown in Fig 16. A pulley was attached to the test bench and the cable was passing through the pulley due to the space restriction of the test bench.

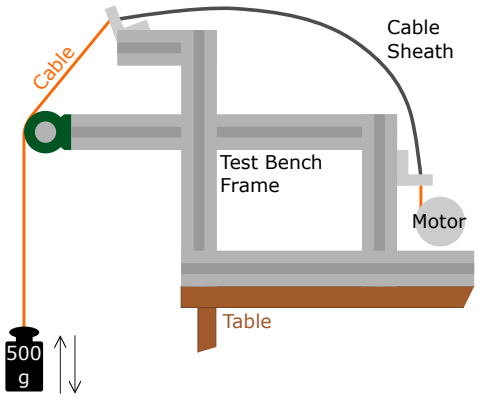

Fig. 16. Test bench setup to obtain a friction compensation model.

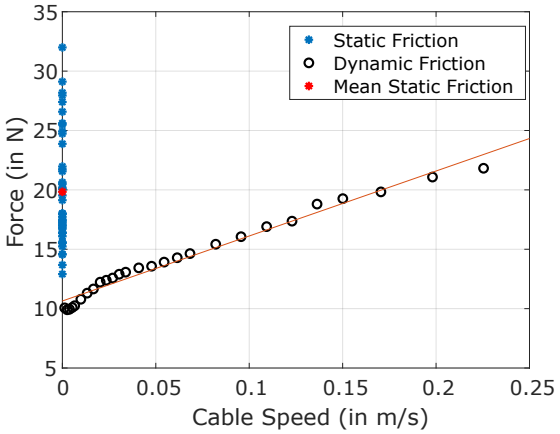

Fig. 17. Friction Compensation Model. The dynamic friction was assumed to be viscous and fitted with the first order equation.

To identify the dynamic friction, the weight was pulled by the motor with various constant speeds from 0.0012 to $0.22\,\mathrm{m/s}$ and the actual current and RPM of the motor were collected simultaneously. Each speed was repeated 25 times and 27 different speeds were applied.

The current of the motor was converted to the motor torque and so was the RPM to the cable pulling speed. The current was mapped with respect to the cable speed and the result is shown in Fig. 17. Because the weight moved with the constant speed, the sum of forces acting on the weight is equal to zero. Thus, the friction torque can be obtained as

$$\sum F_{\text{weight}} = m_{\text{weight}} g + F_{\text{motor}} - F_{\text{friction}} = 0 \qquad (21)$$

where F_{weight} is the force acting on the weight, m_{weight} mass of the weight, g the gravitational acceleration, F_{motor} a cable pulling force from the motor and F_{friction} a dynamic friction force.

Using the mapping, the dynamic friction was assumed to be the first order viscous friction and the compensation model for the dynamic friction was calculated as

$$F_{\text{ff}}(\dot{l}) = 54.71\,\mathrm{kg/s}\ \dot{l} + 10.59\,\mathrm{N} \qquad (22)$$

where F_{ff} is a friction force and $\dot{l}$ is a cable pulling speed.

With regard to static friction, the motor increased its torque until the weight started moving. The current and the speed of the motor were measured and the current at the moment when the weight started moving was considered as the static friction between the cable and the cable sheath. The experiment was repeated 44 times and the result is shown in Fig. 17. The obtained values for the static friction varied a lot during the experiment by the factor of 2.5 approximately. For the static friction model, the mean value of them was used for the compensation model:

$$F_{\text{ff}} = 20\,\mathrm{N} \qquad (23)$$

For the friction compensation model, a corresponding required force for compensation will be added on the top of the control signal out of a PI controller.:

$$F_{ff}(\dot{l}) = \begin{cases} 20\,\mathrm{N}, & \text{if } \dot{l} \leq 0.01\,\mathrm{m/s} \\ 54.71\,\mathrm{kg/s}\ \dot{l} + 10.59\,\mathrm{N}, & \text{otherwise} \end{cases} \qquad (24)$$

where $\dot{l}$ is cable pulling speed. The cable pulling speed was estimated using the velocity of the motor in revolutions per minute.

However, as explained before, the normal force between the cable and the cable sheath varies proportionate to the cable tension therefore the static friction force varies as well. In this experiment, only one weight of $500\,\mathrm{g}$ has been used for the static friction identification. Thus, the friction model does not include for varying static friction forces. In addition, from one exosuit to another, the cable sheath length can differ due to different sizes of the users. It results in requiring different dynamic friction models for different lengths. Due to those artifacts, the output of more sophisticated friction models may not outweigh the effort to obtain them.

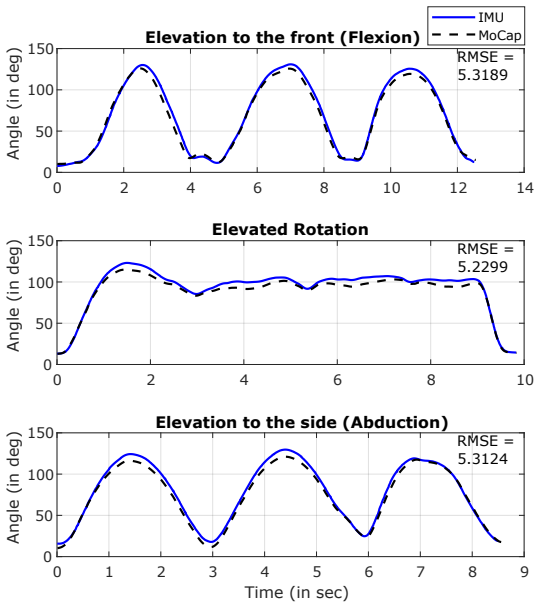

Fig. 18.

Appendix C
Accuracy of IMU

The accuracy of the inertial measurement sensor (IMU) (Hillcrest Laboratories, FSM300) was validated by comparison with the motion capture system (Qualisys, Oqus 300). A sampling frequency of both devices was set to $100\,\mathrm{Hz}$.

One participant was asked to elevate her arm to the front with a comfortable speed and rotate her arm while having her arm elevated around $90°$. Then she was instructed to elevate her arm to the side of her body. The measured data from the both devices are shown in Fig.18. Assuming the motion capture system as the gold standard, the root mean square error (RMSE) was obtained between the two data. For three different motions, the IMU showed consistent performance with the RMSE of $5.3°$.

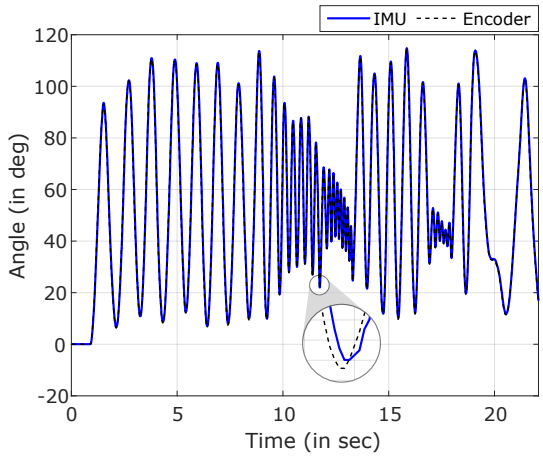

Fig. 19. Angle tracking with a rotary encoder and a inertial measurement unit (IMU). A temporal error between the two measurements was 5 ms

Due to the manual synchronization, the error only can show the spacial error. Thus, the performance of IMU was also compared to a rotary encoder (DFROBOT, SEN0230, 1600 counts/rev) connected to the same microprocessor.

The rotary encoder sampled an elevation angle with 1000 Hz while the IMU with 200 Hz. Considering that the encoder has higher accuracy with shorter delay thus as the gold standard, the delay of 5 ms was observed between the angles measured by each component. Due to the sampling frequency being 200 Hz, the resolution for delay is 5 ms where the cross-correlation was maximum. Therefore, the temporal error of the IMU is 5 ms.

REFERENCES

[1] R. Gopura, D. Bandara, K. Kiguchi, and G. Mann, "Developments in hardware systems of active upper-limb exoskeleton robots: A review," *Robotics and Autonomous Systems*, vol. 75, pp. 203 – 220, 2016. [Online]. Available: http://www.sciencedirect.com/science/article/pii/S0921889015002274

[2] C. T. O'Neill, N. S. Phipps, L. Cappello, S. Paganoni, and C. J. Walsh, "A soft wearable robot for the shoulder: Design, characterization, and preliminary testing," in *2017 International Conference on Rehabilitation Robotics (ICORR)*, July 2017, pp. 1672–1678.

[3] N. Li, T. Yang, P. Yu, J. Chang, L. Zhao, X. Zhao, I. H. Elhajj, N. Xi, and L. Liu, "Bio-inspired upper limb soft exoskeleton to reduce stroke-induced complications," *Bioinspiration & Biomimetics*, vol. 13, no. 6, p. 066001, aug 2018. [Online]. Available: https://doi.org/10.1088%2F1748-3190%2Faad8d4

[4] I. Gaponov, D. Popov, S. J. Lee, and J.-H. Ryu, "Auxilio: A portable cable-driven exosuit for upper extremity assistance," *International Journal of Control, Automation and Systems*, vol. 15, no. 1, pp. 73–84, Feb 2017. [Online]. Available: https://doi.org/10.1007/s12555-016-0487-7

[5] L. Cappello, D. Binh Khanh, S.-C. Yen, and L. Masia, "Design and preliminary characterization of a soft wearable exoskeleton for upper limb," in *2016 6th IEEE International Conference on Biomedical Robotics and Biomechatronics (BioRob)*, June 2016, pp. 623–630.

[6] B. K. Dinh, M. Xiloyannis, C. W. Antuvan, L. Cappello, and L. Masia, "Hierarchical cascade controller for assistance modulation in a soft wearable arm exoskeleton," *IEEE Robotics and Automation Letters*, vol. 2, no. 3, pp. 1786–1793, July 2017.

[7] M. Xiloyannis, D. Chiaradia, A. Frisoli, and L. Masia, "Physiological and kinematic effects of a soft exosuit on arm movements," *Journal of NeuroEngineering and Rehabilitation*, vol. 16, no. 1, p. 29, Feb 2019. [Online]. Available: https://doi.org/10.1186/s12984-019-0495-y

[8] W. Wei, Z. Qu, W. Wang, P. Zhang, and F. Hao, "Design on the bowden cable-driven upper limb soft exoskeleton," *Applied Bionics and Biomechanics*, vol. 2018, pp. 1–9, 07 2018.

[9] J. C. Perry, J. Rosen, and S. Burns, "Upper-limb powered exoskeleton design," *IEEE/ASME Transactions on Mechatronics*, vol. 12, no. 4, pp. 408–417, Aug 2007.

[10] T. G. Sugar, J. He, E. J. Koeneman, J. B. Koeneman, R. Herman, H. Huang, R. S. Schultz, D. E. Herring, J. Wanberg, S. Balasubramanian, P. Swenson, and J. A. Ward, "Design and control of rupert: A device for robotic upper extremity repetitive therapy," *IEEE Transactions on Neural Systems and Rehabilitation Engineering*, vol. 15, no. 3, pp. 336–346, Sep. 2007.

[11] S. Balasubramanian, , M. Perez, B. Shepard, E. Koeneman, and J. K. and, "Rupert: An exoskeleton robot for assisting rehabilitation of arm functions," in *2008 Virtual Rehabilitation*, Aug 2008, pp. 163–167.

[12] T. Nef, M. Guidali, and R. Riener, "ARMin III - Arm Therapy Exoskeleton with an Ergonomic Shoulder Actuation," *Applied Bionics and Biomechanics*, vol. 6, pp. 127–142, 01 2009.

[13] M. A. Ergin and V. Patoglu, "Assiston-se: A self-aligning shoulder-elbow exoskeleton," in *2012 IEEE International Conference on Robotics and Automation*, May 2012, pp. 2479–2485.

[14] A. Otten, C. Voort, A. Stienen, R. Aarts, E. van Asseldonk, and H. van der Kooij, "Limpact:a hydraulically powered self-aligning upper limb exoskeleton," *IEEE/ASME Transactions on Mechatronics*, vol. 20, no. 5, pp. 2285–2298, Oct 2015.

[15] R. Farris, H. Quintero, and M. Goldfarb, "Preliminary evaluation of a powered lower limb orthosis to aid walking in paraplegic individuals," *IEEE transactions on neural systems and rehabilitation engineering : a publication of the IEEE Engineering in Medicine and Biology Society*, vol. 19, pp. 652–9, 12 2011.

[16] N. Jarrasse and G. Morel, "Connecting a human limb to an exoskeleton," *IEEE Transactions on Robotics*, vol. 28, no. 3, pp. 697–709, June 2012.

[17] D. of Economic and P. D. Social Affairs, "World population ageing 2017 (st/esa/ser.a/408)," 2017.

[18] H. Kobayashi and H. Nozaki, "Development of muscle suit for supporting manual worker," in *2007 IEEE/RSJ International Conference on Intelligent Robots and Systems*, Oct 2007, pp. 1769–1774.

[19] D. Park and K.-J. Cho, "Development and evaluation of a soft wearable weight support device for reducing muscle fatigue on shoulder," *PLOS ONE*, vol. 12, no. 3, pp. 1–24, 03 2017. [Online]. Available: https://doi.org/10.1371/journal.pone.0173730

[20] Y. G. Kim, M. Xiloyannis, D. Accoto, and L. Masia, "Development of a soft exosuit for industrial applications," in *2018 7th IEEE International Conference on Biomedical Robotics and Biomechatronics (Biorob)*, Aug 2018, pp. 324–329.

[21] C. Majidi, "Soft robotics : A perspective - current trends and prospects for the future," 2013.

[22] Y. Mao and S. K. Agrawal, "Design of a cable-driven arm exoskeleton (carex) for neural rehabilitation," *IEEE Transactions on Robotics*, vol. 28, no. 4, pp. 922–931, Aug 2012.

[23] G. Wu, F. C. van der Helm, H. D. Veeger, M. Makhsous, P. V. Roy, C. Anglin, J. Nagels, A. R. Karduna, K. McQuade, X. Wang, F. W. Werner, and B. Buchholz, "Isb recommendation on definitions of joint coordinate systems of various joints for the reporting of human joint motion-part ii: shoulder, elbow, wrist and hand," *Journal of Biomechanics*, vol. 38, no. 5, pp. 981 – 992, 2005. [Online]. Available: http://www.sciencedirect.com/science/article/pii/S002192900400301X

[24] B. S. Rupal, S. Rafique, A. Singla, E. Singla, M. Isaksson, and G. S. Virk, "Lower-limb exoskeletons: Research trends and regulatory guidelines in medical and non-medical applications," *International Journal of Advanced Robotic Systems*, vol. 14, no. 6, p. 1729881417743554, 2017. [Online]. Available: https://doi.org/10.1177/1729881417743554

[25] D. Magermans, E. Chadwick, H. Veeger, and F. van der Helm, "Requirements for upper extremity motions during activities of daily living," *Clinical Biomechanics*, vol. 20, no. 6, pp. 591 – 599, 2005. [Online]. Available: http://www.sciencedirect.com/science/article/pii/S0268003305000434

[26] C. J. van Andel, N. Wolterbeek, C. A. Doorenbosch, D. H. Veeger, and J. Harlaar, "Complete 3d kinematics of upper extremity functional tasks," *Gait & Posture*, vol. 27, no. 1, pp. 120 – 127, 2008. [Online]. Available: http://www.sciencedirect.com/science/article/pii/S0966636207000665

[27] J. Aizawa, T. Masuda, T. Koyama, K. Nakamaru, K. Isozaki, A. Okawa, and S. Morita, "Three-dimensional motion of the upper extremity joints during various activities of daily living," *Journal of Biomechanics*, vol. 43, no. 15, pp. 2915 – 2922, 2010. [Online]. Available: http://www.sciencedirect.com/science/article/pii/S0021929010003878

[28] D. H. Gates, L. S. Walters, J. Cowley, J. M. Wilken, and L. Resnik, "Range of motion requirements for upper-limb activities of daily living," *American Journal of Occupational Therapy*, vol. 70,

no. 1, pp. 7 001 350 010p1–7 001 350 010p10, 2015. [Online]. Available: +http://dx.doi.org/10.5014/ajot.2016.015487

[29] S. M. Engdahl and D. H. Gates, "Reliability of upper limb and trunk joint angles in healthy adults during activities of daily living," *Gait & Posture*, vol. 60, pp. 41 – 47, 2018. [Online]. Available: http://www.sciencedirect.com/science/article/pii/S0966636217309864

[30] F. Fayad, G. Hoffmann, S. Hanneton, C. Yazbeck, M. Lefevre-colau, S. Poiraudeau, M. Revel, and A. Roby-Brami, "3-d scapular kinematics during arm elevation: Effect of motion velocity," *Clinical Biomechanics*, vol. 21, no. 9, pp. 932 – 941, 2006. [Online]. Available: http://www.sciencedirect.com/science/article/pii/S0268003306000908

[31] T. Flash and N. Hogan, "The coordination of arm movements: an experimentally confirmed mathematical model," *Journal of Neuroscience*, vol. 5, no. 7, pp. 1688–1703, 1985. [Online]. Available: https://www.jneurosci.org/content/5/7/1688

[32] I. A. Murray and G. R. Johnson, "A study of the external forces and moments at the shoulder and elbow while performing every day tasks," *Clinical Biomechanics*, vol. 19, no. 6, pp. 586 – 594, 2004. [Online]. Available: http://www.sciencedirect.com/science/article/pii/S0268003304000531

[33] D. Chen, Y. Yun, and A. D. Deshpande, "Experimental characterization of bowden cable friction," in *2014 IEEE International Conference on Robotics and Automation (ICRA)*, May 2014, pp. 5927–5933.

[34] B. K. Dinh, M. Xiloyannis, L. Cappello, C. W. Antuvan, S.-C. Yen, and L. Masia, "Adaptive backlash compensation in upper limb soft wearable exoskeletons," *Robotics and Autonomous Systems*, vol. 92, pp. 173 – 186, 2017. [Online]. Available: http://www.sciencedirect.com/science/article/pii/S0921889016303591

[35] H. Kazerooni, J. . Racine, Lihua Huang, and R. Steger, "On the control of the berkeley lower extremity exoskeleton (bleex)," in *Proceedings of the 2005 IEEE International Conference on Robotics and Automation*, April 2005, pp. 4353–4360.

[36] S. Balasubramanian, A. Melendez-Calderon, A. Roby-Brami, and E. Burdet, "On the analysis of movement smoothness," *Journal of NeuroEngineering and Rehabilitation*, vol. 12, no. 1, p. 112, Dec 2015. [Online]. Available: https://doi.org/10.1186/s12984-015-0090-9

[37] T. Do, T. Tjahjowidodo, M. Lau, and S. Phee, "An investigation of friction-based tendon sheath model appropriate for control purposes," *Mechanical Systems and Signal Processing*, vol. 42, no. 1, pp. 97 – 114, 2014. [Online]. Available: http://www.sciencedirect.com/science/article/pii/S0888327013003890

[38] T. R. Farrell and R. F. Weir, "The optimal controller delay for myoelectric prostheses," *IEEE Transactions on Neural Systems and Rehabilitation Engineering*, vol. 15, no. 1, pp. 111–118, March 2007.

[39] A. Calanca, R. Muradore, and P. Fiorini, "A review of algorithms for compliant control of stiff and fixed-compliance robots," *IEEE/ASME Transactions on Mechatronics*, vol. 21, no. 2, pp. 613–624, April 2016.

[40] G. Lee, Y. Ding, I. G. Bujanda, N. Karavas, Y. M. Zhou, and C. J. Walsh, "Improved assistive profile tracking of soft exosuits for walking and jogging with off-board actuation," in *2017 IEEE/RSJ International Conference on Intelligent Robots and Systems (IROS)*, Sep. 2017, pp. 1699–1706.